

1 **Requirement for STAT3 and its target, TFCP2L1, in self-renewal of naïve pluripotent stem**
2 **cells *in vivo* and *in vitro***

3
4 Sophie Kraunsoe^{1,2,5}, Takuya Azami^{1,4}, Yihan Pei^{1,2}, Graziano Martello⁶, Kenneth Jones^{1,7},
5 Thorsten Boroviak^{2,3}, and Jennifer Nichols^{1,2,3,4*}

6
7 **Affiliations**

8 ¹Wellcome Trust – Medical Research Council Stem Cell Institute, University of Cambridge, Jeffrey
9 Cheah Biomedical Centre, Puddicombe Way, Cambridge CB2 0AW, UK

10 ²Department of Physiology, Development and Neuroscience, University of Cambridge, Tennis
11 Court Road, Cambridge CB2 3EG, UK

12 ³Centre for Trophoblast Research, University of Cambridge, UK

13 ⁴Current address: MRC Human Genetics Unit, Institute of Genetics and Cancer, University of
14 Edinburgh, Western General Hospital, Crewe Road South, Edinburgh EH4 2XU, UK

15 ⁵School of Bioscience, University of Nottingham Sutton Bonington Campus, Loughborough, LE12
16 5RD, UK

17 ⁶Department of Biology, University of Padua, Italy

18 ⁷Current address: Department of Biochemistry, University of Cambridge

19 *Author for correspondence

20 Jenny.nichols@ed.ac.uk

21

22 **Key words**

23 Naïve pluripotency

24 Embryonic diapause

25 STAT3

26 TFCP2L1

27 Blastocyst

28 Embryonic stem cells

29

30 **Summary Statement**

31 Inducing diapause in mouse embryos demonstrates that STAT3 and TFCP2L1 are essential for
32 self-renewal of the epiblast, but only TFCP2L1 is required for derivation of embryonic stem cells.

33 **Abstract**

34 We previously demonstrated gradual loss of epiblast during diapause in embryos lacking
35 components of the LIF/IL6 receptor. Here we explore requirement for the downstream signalling
36 transducer and activator of transcription, STAT3 and its target, TFCP2L1, in maintenance of naïve
37 pluripotency. Unlike conventional markers, such as NANOG, which remains high in epiblast until
38 implantation, both STAT3 and TFCP2L1 proteins decline during blastocyst expansion, but intensify
39 in the embryonic region after induction of diapause, as observed visually and confirmed using our
40 novel image analysis tool, consistent with our previous transcriptional expression data. Embryos
41 lacking STAT3 or TFCP2L1, underwent catastrophic loss of most of the inner cell mass during the
42 first few days of diapause, implicating involvement of signals in addition to LIF/IL6 for sustaining
43 naïve pluripotency *in vivo*. By blocking MEK/ERK signalling from the morula stage we could derive
44 embryonic stem cells with high efficiency from STAT3 null embryos, but not those lacking
45 TFCP2L1, suggesting a hitherto unknown additional role for this essential STAT3 target in
46 transition from embryo to embryonic stem cells *in vitro*.

47

48

49 **Introduction**

50 Embryonic stem cell lines (ESCs) derived from epiblasts of preimplantation mouse embryos
51 (Evans and Kaufman, 1981; Martin, 1981) have been used extensively to study and model
52 mammalian development, since they can be expanded in culture, whilst retaining the ability to
53 differentiate into all tissues of the body. This flexible state is known as 'naïve pluripotency' (Nichols
54 and Smith, 2009). ESCs can self-renew in medium supplemented with leukaemia inhibitory factor
55 (LIF) (Smith et al., 1988; Williams et al., 1988), operating via signal transducer and activator of
56 transcription (STAT)3 (Burdon et al., 1999; Matsuda et al., 1999; Niwa et al., 1998). The LIF
57 receptor complex comprising LIFR and gp130 (also known as IL6ST) activates Janus-associated
58 kinases (JAKs), which phosphorylate STAT3 at tyrosine 705 (pY705) (Ni et al., 2004; Zhang et al.,
59 2000). Mutation of pY705 ablates ESC self-renewal in standard (serum/LIF) culture conditions
60 (Huang et al., 2014); LIF or related cytokines were therefore previously considered essential for
61 ESC self-renewal. However, a refined serum-free culture regime, '2i', based upon dual inhibition of
62 Glycogen Synthase Kinase (GSK)3 and MEK/ERK, allows ESC derivation from STAT3 mutant
63 embryos by incubation from the morula stage (Ying et al., 2008). STAT3 null ESCs enabled
64 analysis of downstream signalling events associated with ESC self-renewal, and thus
65 characterisation of the signalling network operative during maintenance of naïve pluripotency *in*
66 *vitro* (Martello et al., 2013; Ye et al., 2013). The most significant player emerging from this analysis
67 was TFCEP2L1 (also known as CRTR-1) whose forced expression could rescue STAT3 null ESCs
68 in serum/LIF culture. Using pathway analysis and computational modelling an essential role for
69 TFCEP2L1 in ESC maintenance was proposed and supported experimentally (Dunn et al., 2014).
70 Moreover, transfection of *Tfcp2l1* into epiblast stem cells (EpiSCs) derived from postimplantation
71 epiblasts (Brons et al., 2007; Tesar et al., 2007) could direct reprogramming from primed to naïve
72 pluripotency, confirming participation of TFCEP2L1 in the naïve pluripotency network (Martello et al.,
73 2013; Ye et al., 2013).

74 Combined maternal and zygotic deletion revealed an essential requirement for STAT3
75 during blastocyst expansion, confirming its suspected function in epiblast formation (Do et al.,
76 2013). However, perdurance of maternal STAT3 protein in zygotic null embryos permits
77 developmental progression beyond cleavage stages, allowing them to implant in the uterus, where

78 they acquire abnormalities (Takeda et al., 1997). Interestingly, mutation of either LIFR or gp130
79 results in considerably less severe phenotypes (Li et al., 1995; Yoshida et al., 1996), supporting
80 previous suggestions of additional alternative requirement for STAT3 signalling in early mouse
81 development (Kristensen et al., 2005).

82 In normal laboratory rodents, the state of naïve pluripotency is relatively transient, lasting
83 no more than two days. It is therefore debatable whether self-renewal of naïve pluripotent stem
84 cells occurs at this stage during uninterrupted development. Conveniently, murine preimplantation
85 embryogenesis can be prolonged by diapause, a natural, facultative phenomenon ensuing when a
86 dam conceives whilst suckling a previous litter. Embryos progress to the periimplantation stage,
87 embryonic day (E)4.5, but delay implantation until a source of oestrogen is regained. Diapause can
88 be achieved experimentally by ovariectomy prior to the physiological burst of oestrogen secretion
89 at E2.5 (Weitlauf and Greenwald, 1968). Healthy blastocysts are able to sustain diapause for more
90 than a month, then resume normal development (Arena et al., 2021). In previous studies, we
91 showed that epiblast in diapause embryos lacking LIFR or gp130 was gradually reduced by
92 apoptosis, leaving only trophectoderm and primitive endoderm (PrE) (Nichols et al., 2001). Loss of
93 STAT3 or its target, TFCEP2L1, may be anticipated to result in a more dramatic phenotype. Here we
94 show that both STAT3 and TFCEP2L1 are critically required for diapause, with almost complete loss
95 of both epiblast and PrE comprising the inner cell mass (ICM) occurring within 4 days of diapause
96 onset (6 days after ovariectomy). Although both pY705 STAT3 and TFCEP2L1 are downregulated in
97 the epiblast before implantation, their levels intensify during diapause, consistent with previously
98 published RNA profiling (Boroviak et al., 2015). To enhance optical compartmentalisation of tissue
99 types in periimplantation and diapause embryos, we developed an image analysis tool to quantify
100 confocal readout of protein levels and distribution for pY705 STAT3 and TFCEP2L1. Despite the
101 rapid loss of epiblast in diapaused mutant embryos, we show that capture of self-renewing ESCs
102 from STAT3 null embryos in culture is as efficient as from wild type and heterozygous embryos. In
103 contrast, no ESCs could be derived from embryos lacking TFCEP2L1, implicating alternative
104 functions for this factor in replication of naïve pluripotent epiblast cells that is not directed by
105 STAT3 signalling.

106

107 **Results**

108 *STAT3 pY705 and TFCP2L1 peak in epiblast during embryonic diapause*

109 The potential roles of STAT3 and TFCP2L1 in sustaining pluripotency *in vivo* were investigated via
110 induction of diapause (Fig.1A), as described previously (Nichols et al., 2001). Bilateral ovariectomy
111 was performed on female CD1 mice 2.5 days after mating by males of the same strain. Embryos
112 were flushed 6 days later, and were therefore in the state of diapause for 4 days.
113 Immunofluorescence (IF) using antibodies raised against NANOG, STAT3 (pY705) and TFCP2L1
114 was performed using our standard protocol (Silva et al., 2009), but with methanol permeabilization,
115 on non-diapaused embryos at E3.5 and 4.5 and following 4 days of diapause (Fig.1B).
116 Quantification for levels of NANOG, pY705 and TFCP2L1 proteins in the embryonic region was
117 enabled by manual cropping to exclude the abembryonic, mural trophoctoderm region (Fig.2A),
118 and application of a novel image analysis tool (Fig.2B). In concordance with visual appearance of
119 the confocal images, a significant increase of both pY705 and TFCP2L1 IF was quantified in
120 diapause epiblast compared with non-diapaused periimplantation embryos at E4.5 (Fig.2C),
121 consistent with mRNA levels and the transcriptional resemblance of diapause epiblast to self-
122 renewing ESCs *in vitro* (Boroviak et al., 2015). During manual cropping of the images analysed
123 with the image analysis tool, most mural trophoctoderm was removed to prevent these cells
124 confounding the analysis. By creating spatially reconstructed *in silico* embryos, it can be observed
125 that cells selected for high levels of STAT3 pY705 or TFCP2L1 are enriched in the epiblast
126 compartment of diapaused embryos (Fig.3A,B). In contrast, E4.5 embryos have lower levels of
127 STAT3 pY705 in their epiblast compartment compared to E3.5 and diapaused embryos (Fig3C).

128

129 *Propagation of naïve pluripotency in vivo requires STAT3 and TFCP2L1*

130 To assess functionality of STAT3 signalling during maintenance of naïve pluripotency,
131 heterozygous mice were mated *inter se* to generate wild type (WT), heterozygous (het) and mutant
132 (null) embryos for *Stat3* or *Tfcp2l1*. Diapause embryos were recovered 6 days after ovariectomy
133 and IF for NANOG, pY705 and TFCP2L1 was performed. Whereas WT and het embryos
134 possessed large ICMs with many NANOG, pY705 and TFCP2L1 positive cells, embryos lacking
135 STAT3 or TFCP2L1 exhibited complete loss or severe reduction of the whole ICM (Fig.4A,B). In

136 both cases, null embryos were underrepresented (Fig.4C), probably attributed to loss before
137 retrieval owing to catastrophic reduction of the ICM impacting on trophectoderm expansion and
138 embryo integrity. Taken together, these results implicate immediate requirement for STAT3
139 signalling and functional TFCP2L1 during diapause.

140

141 *Capture of ESCs from embryos*

142 Our previous derivation protocol based upon blocking MEK/ERK and GSK3 from the morula stage
143 of development (Ying et al., 2008) was used to capture CD1 background ESCs. 41 WT or het and
144 13 null ESC lines were generated from 56 embryos by *inter se* mating of *Stat3* het mice (Table 1).
145 Each embryo was genotyped by PCR using lysed trophectoderm produced during immunosurgery
146 (Nichols et al., 1998; Solter and Knowles, 1975). *Stat3* null lines were confirmed by genotyping
147 after expansion. *Stat3* null and WT cell lines could be propagated indistinguishably in 2i medium
148 (Fig.4D) and no distinct difference in cell cycle kinetics could be perceived between them (Fig.4E).
149 IF for OCT4 and NANOG confirmed naïve pluripotent identity for both WT and STAT3 null ESC
150 lines (Fig.4F). Conversely, from 65 morulae generated from *Tfcp2l1* het inter-cross, 6 WT and 49
151 het, but no null ESC lines were derived from 65 embryos (Table 1), suggesting a distinct
152 requirement for TFCP2L1 in capture of pluripotency *in vitro*.

153

154 **Discussion**

155 Derivation of *Stat3* null ESCs previously facilitated interrogation of STAT3 targets and highlighted
156 TFCEP2L1 as the most significant *in vitro* (Martello et al., 2013; Ying et al., 2008). To investigate the
157 potential role of STAT3 and TFCEP2L1 in maintenance of naïve pluripotency *in vivo* we induced
158 embryonic diapause. IF for pSTAT3(Y705), the protein product utilised for self-renewal of ESCs
159 (Huang et al., 2014), and TFCEP2L1 both become visibly enriched in the epiblast during diapause
160 (Fig.1). This observation was validated using a novel tool developed for quantification of IF images
161 of tightly compacted nuclei (Figs.2-3), thus implying a possible role for these factors for epiblast
162 self-renewal *in vivo*. During diapause, in contrast to the phenotype observed following deletion of
163 LIFR or its co-receptor, gp130, which resulted in gradual loss of epiblast, but not PrE (Nichols et
164 al., 2001), embryos lacking either STAT3 or TFCEP2L1 lost virtually the entire ICM within only a few
165 days (Fig.4). This more dramatic phenotype may be a consequence of the precipitous depletion of
166 epiblast, the source of PrE-inducing FGF4 (Yamanaka et al., 2010), compared with deletion of LIF
167 receptor complex components (Nichols et al., 2001). STAT3 also promotes anti-apoptotic activity
168 (Hirano et al., 2000), which could contribute to the enhanced PrE population reported in
169 blastocysts supplemented with IL6 (Anderson et al., 2017; Morgani and Brickman, 2015). We
170 conclude that STAT3 signalling is essential to maintain naïve pluripotency *in vivo* and operates as
171 a signal transducer for pathways in addition to that induced by IL6 family cytokines.

172 Interestingly, we recently found precocious expression of PrE markers such as *Pdgrfa*,
173 *Sox17* and *Gata4* in *Stat3* null embryos at the mid blastocyst stage (E3.5), whereas emerging
174 epiblast cells at E3.75 prematurely activated the postimplantation epiblast genes *Utf1*, *Otx2* and its
175 targets *Dnmt3a* and *b* (Betto et al., 2021), which presumably instigated reduction of FGF4
176 secretion. However, previous observations of PrE persistence during diapause when LIFR or
177 gp130 are deleted (Nichols et al., 2001) imply independence of this branch of STAT3 signalling for
178 PrE maintenance. The present data implicate STAT3 signalling, via TFCEP2L1, in PrE maintenance
179 *in vivo*. Our failure to derive ESCs from *Tfcp2l1* null embryos using the strategy that proved highly
180 successful for generation of *Stat3* null ESCs (Table 1) implies an unexpected STAT3-independent
181 role for TFCEP2L1 in transition towards *in vitro* self-renewal of pluripotent stem cells. TFCEP2L1
182 plays a role in upregulation of *Nanog* (Ye et al., 2013), which is also indispensable for derivation of

183 ESCs from mouse embryos (Silva et al., 2009). Interestingly, both *Nanog* and *Tfcp2l1* can be
184 deleted from established ESCs cultured in 2i/LIF (Chambers et al., 2007; Martello et al., 2013; Yan
185 et al., 2021), implicating compensation by the robust and redundant network of pluripotency factors
186 assembled in ESCs *in vitro* (Dunn et al., 2014). This pathway connection may explain the failure of
187 embryos lacking TFPC2L1 to yield ESCs and further highlights the distinct requirements for self-
188 renewal of naïve pluripotent cells *in vivo* compared with established cell lines *in vitro*.
189

190 **Materials and Methods**

191 *Mice, husbandry and embryos*

192 Experiments were performed in accordance with EU guidelines for the care and use of laboratory
193 animals and under the authority of appropriate UK governmental legislation. Use of animals in this
194 project was approved by the Animal Welfare and Ethical Review Body for the University of
195 Cambridge and relevant Home Office licences are in place.

196 Mice were maintained on a lighting regime of 12:12 hours light:dark with food and water supplied
197 *ad libitum*. *Stat3* mice heterozygous for replacement of exons 20-22 with Neomycin resistance
198 (Takeda et al., 1997) were backcrossed to CD1 mice. *Tfcp2l1* heterozygous mice were generated
199 from ESCs targeted using CRISPR strategy in E14 ESCs obtained from Jackson Labs Knockout
200 Mouse Project (KOMP), via injection into C57BL/6 blastocysts to generate chimaeras. Male
201 chimaeras were mated with CD1 females; grey pups were genotyped by PCR of ear biopsies and
202 robust males selected for further backcrossing to CD1 females. Both STAT3 and TFCEP2L1 mouse
203 lines were maintained by backcrossing to CD1. Embryos were generated from *Stat3*^{+/-} or *Tfcp2l1*^{+/-}
204 *inter se* natural mating. Detection of a copulation plug in the morning after mating indicated
205 embryonic day (E)0.5. Embryos were isolated in M2 medium (Sigma-Aldrich).

206

207 *Genotyping*

208 Mice were genotyped by PCR using ear biopsies collected within 4 weeks of birth and genomic
209 DNA was extracted using Extract-N-Amp tissue prep kit (Sigma-Aldrich). Embryos were genotyped
210 using either immune-reactivity to antibody raised against either STAT3 pY705 or TFCEP2L1 in the
211 case of those imaged for confocal analysis, or PCR analysis of trophectoderm lysate for ESC
212 derivation. Amplification was carried out on 5 µL of lysate for 35 cycles (following 95°C hot start for
213 10 minutes) of 94°C, 15 seconds; 60°C, 12 seconds; 72°C, 60 seconds, with a final extension at
214 72°C for 10 minutes. Reaction products were resolved by agarose gel electrophoresis. Primers
215 used for genotyping PCR are listed in Table.S1.

216

217 *Induction of diapause*

218 To determine the requirement for STAT3 or TFCP2L1 during maintenance of the embryo during
219 delayed implantation, CD1 females or het females mated by het males were surgically
220 ovariectomised under general anaesthesia as described previously (Nichols et al., 2001) before the
221 embryos reached E2.5. Diapause embryos were flushed 6 days later and fixed for IF.

222

223 *Derivation and culture of ESC lines*

224 Morulae were collected from het females 2.5 days after mating by het males and used for ESC
225 derivation as described previously (Ying et al., 2008) by culture to the blastocyst stage in KSOM
226 supplemented with 2i, consisting of 1 μ M PD0325901 and 3 μ M CHIR99021, transfer of ICMs
227 isolated by immunosurgery (Solter and Knowles, 1975) to 48-well plates containing 2i in N2B27
228 medium, one per well. WT and *Stat3* null ESCs were expanded and maintained in N2B27
229 supplemented with 2i or 2i/LIF on gelatin-coated plates at 37°C in 7% CO₂ and passaged by
230 enzymatic disaggregation every 2-3 days.

231

232 *Immunofluorescence (IF)*

233 Embryos were fixed in 4% paraformaldehyde (PFA) for 30 min at room temperature (RT), followed
234 by washing in 0.5% polyvinylpyrrolidone (PVP) in PBS. Embryos were permeabilized in 0.5%
235 Triton X-100 in PBS for 15 min and blocked with 2% donkey serum, 2.5% BSA, and 0.1%
236 Tween20 in PBS (blocking solution) for 1 h at RT. For phosphorylated-STAT3 staining,
237 permeabilization was performed in absolute methanol for 10 min at -20°C. Primary antibodies were
238 diluted in blocking solution and embryos incubated in these overnight at 4°C. After washing in 0.1%
239 Tween 20 in PBS, embryos were incubated with Alexa Fluor-conjugated secondary antibodies
240 (Thermo) at 1:500 dilution in blocking solution for 1 h at RT. Nuclear staining was carried out with
241 Hoechst33342 or DAPI (Thermo). Primary and secondary antibodies used are listed in Table S2.

242

243 *Imaging and image analysis of embryos*

244 Images for embryos were acquired using TCS SP5 (Leica) confocal microscope and processed
245 with ImageJ. Quantification of IF images was achieved using a computational pipeline to extract
246 data on the intensity of antibody staining in individual nuclei. The 2D StarDist segmentation Fiji

247 plugin (parameters: 'percentileBottom': '1.0', 'percentileTop': '99.9', 'probThresh': '0.2',
248 'nmsThresh': '0.2') was used to segment the DNA channel of IF images before using the Trackmate
249 plugin to 'track' objects through the z-stack to generate 3D objects (parameters: area threshold >
250 5, <30, track duration > 5) (Ershov et al., 2022). An unsharp mask was applied to the DNA channel
251 prior to segmentation (parameters: radius = 15, mask = 0.6). Nuclear segmentation of embryos
252 was used as a mask to measure fluorescence intensity, xyz position, and morphological
253 parameters (e.g., volume) of each nucleus (Ollion et al., 2013; Pietzsch et al., 2015). Assessment
254 of the histograms for signal intensity in the DNA channel and nuclear volume allowed thresholds to
255 be set to remove erroneously segmented nuclei. Violin plots were generated using the ggplot2
256 package in R and statistical significance between embryo groups was assessed via pair-wise
257 unpaired student's t-tests. Nuclei were visualised in a 2D gene expression space based on
258 NANOG and STAT3 intensity and selected nuclei were plotted back into the 'in silico' embryos,
259 based on their positional information and colour coded by STAT3 expression levels. 'In silico'
260 embryos were generated using xyz centroid information from the segmentation mask and colour
261 coded according to STAT3 intensity.

262

263 *Acknowledgements*

264 We wish to thank William Mansfield for generation of Tfcp2l1+/- mouse line; Shizuo Akira for
265 providing Stat3+/- mice; Peter Humphreys and Darran Clement for advanced imaging and
266 analysis; UBS, Cambridge for animal husbandry.

267

268 No competing interests declared

269

270 *Funding*

271 This work was supported by the University of Cambridge, BBSRC project grant RG74277 and
272 funded in part by Wellcome Trust (Grant number: 203151/Z/16/Z). T.A. is supported by JSPS
273 Overseas Research Fellowship and UEHARA Memorial Foundation Fellowship.

274 For the purpose of Open Access, the author has applied a CC BY public copyright licence to any

275 Author Accepted Manuscript version arising from this submission.

276 *Data Availability*

277 Fiji macro and R codes will be made available at

278 https://github.com/SKraunsoe/STAT3_embryo_segmentation_analysis

279

280

281 References

- 282 **Anderson, K. G. V., Hamilton, W. B., Roske, F. V., Azad, A., Knudsen, T. E., Canham, M. A.,**
283 **Forrester, L. M. and Brickman, J. M.** (2017). Insulin fine-tunes self-renewal pathways
284 governing naive pluripotency and extra-embryonic endoderm. *Nat Cell Biol* **19**, 1164-1177.
- 285 **Arena, R., Bisogno, S., Gasior, L., Rudnicka, J., Bernhardt, L., Haaf, T., Zacchini, F., Bochenek, M.,**
286 **Fic, K., Bik, E., et al.** (2021). Lipid droplets in mammalian eggs are utilized during embryonic
287 diapause. *Proc Natl Acad Sci U S A* **118**.
- 288 **Betto, R. M., Diamante, L., Perrera, V., Audano, M., Rapelli, S., Lauria, A., Incarnato, D., Arboit,**
289 **M., Pedretti, S., Rigoni, G., et al.** (2021). Metabolic control of DNA methylation in naive
290 pluripotent cells. *Nat Genet.*
- 291 **Boroviak, T., Loos, R., Lombard, P., Okahara, J., Behr, R., Sasaki, E., Nichols, J., Smith, A. and**
292 **Bertone, P.** (2015). Lineage-Specific Profiling Delineates the Emergence and Progression of
293 Naive Pluripotency in Mammalian Embryogenesis. *Dev Cell* **35**, 366-382.
- 294 **Brons, I. G., Smithers, L. E., Trotter, M. W., Rugg-Gunn, P., Sun, B., Chuva de Sousa Lopes, S. M.,**
295 **Howlett, S. K., Clarkson, A., Ahrlund-Richter, L., Pedersen, R. A., et al.** (2007). Derivation
296 of pluripotent epiblast stem cells from mammalian embryos. *Nature* **448**, 191-195.
- 297 **Burdon, T., Stracey, C., Chambers, I., Nichols, J. and Smith, A.** (1999). Suppression of SHP-2 and
298 ERK signalling promotes self-renewal of mouse embryonic stem cells. *Dev Biol* **210**, 30-43.
- 299 **Chambers, I., Silva, J., Colby, D., Nichols, J., Nijmeijer, B., Robertson, M., Vrana, J., Jones, K.,**
300 **Grotewold, L. and Smith, A.** (2007). Nanog safeguards pluripotency and mediates germline
301 development. *Nature* **450**, 1230-1234.
- 302 **Do, D. V., Ueda, J., Messerschmidt, D. M., Lorthongpanich, C., Zhou, Y., Feng, B., Guo, G., Lin, P.**
303 **J., Hossain, M. Z., Zhang, W., et al.** (2013). A genetic and developmental pathway from
304 STAT3 to the OCT4-NANOG circuit is essential for maintenance of ICM lineages in vivo.
305 *Genes Dev* **27**, 1378-1390.
- 306 **Dunn, S. J., Martello, G., Yordanov, B., Emmott, S. and Smith, A. G.** (2014). Defining an essential
307 transcription factor program for naive pluripotency. *Science* **344**, 1156-1160.
- 308 **Ershov, D., Phan, M. S., Pylvanainen, J. W., Rigaud, S. U., Le Blanc, L., Charles-Orszag, A.,**
309 **Conway, J. R. W., Laine, R. F., Roy, N. H., Bonazzi, D., et al.** (2022). TrackMate 7:
310 integrating state-of-the-art segmentation algorithms into tracking pipelines. *Nat Methods*
311 **19**, 829-832.
- 312 **Evans, M. J. and Kaufman, M.** (1981). Establishment in culture of pluripotential cells from mouse
313 embryos. *Nature* **292**, 154-156.
- 314 **Hirano, T., Ishihara, K. and Hibi, M.** (2000). Roles of STAT3 in mediating the cell growth,
315 differentiation and survival signals relayed through the IL-6 family of cytokine receptors.
316 *Oncogene* **19**, 2548-2556.
- 317 **Huang, G., Yan, H., Ye, S., Tong, C. and Ying, Q. L.** (2014). STAT3 phosphorylation at tyrosine 705
318 and serine 727 differentially regulates mouse ESC fates. *Stem Cells* **32**, 1149-1160.
- 319 **Kristensen, D. M., Kalisz, M. and Nielsen, J. H.** (2005). Cytokine signalling in embryonic stem cells.
320 *APMIS* **113**, 756-772.
- 321 **Li, M., Sendtner, M. and Smith, A.** (1995). Essential function of LIF receptor in motor neurons.
322 *Nature* **378**, 724-727.
- 323 **Martello, G., Bertone, P. and Smith, A.** (2013). Identification of the missing pluripotency mediator
324 downstream of leukaemia inhibitory factor. *EMBO J.*
- 325 **Martin, G. R.** (1981). Isolation of a pluripotent cell line from early mouse embryos cultured in
326 medium conditioned by teratocarcinoma stem cells. *Proc. Natl. Acad. Sci. USA* **78**, 7634-
327 7638.

- 328 **Matsuda, T., Nakamura, T., Nakao, K., Arai, T., Katsuki, M., Heike, T. and Yokota, T.** (1999). STAT3
329 activation is sufficient to maintain an undifferentiated state of mouse embryonic stem
330 cells. *Embo J* **18**, 4261-4269.
- 331 **Morgani, S. M. and Brickman, J. M.** (2015). LIF supports primitive endoderm expansion during
332 pre-implantation development. *Development* **142**, 3488-3499.
- 333 **Ni, C. W., Hsieh, H. J., Chao, Y. J. and Wang, D. L.** (2004). Interleukin-6-induced JAK2/STAT3
334 signaling pathway in endothelial cells is suppressed by hemodynamic flow. *Am J Physiol Cell*
335 *Physiol* **287**, C771-780.
- 336 **Nichols, J., Chambers, I., Taga, T. and Smith, A.** (2001). Physiological rationale for responsiveness
337 of mouse embryonic stem cells to gp130 cytokines. *Development* **128**, 2333-2339.
- 338 **Nichols, J. and Smith, A.** (2009). Naive and primed pluripotent states. *Cell Stem Cell* **4**, 487-492.
- 339 **Nichols, J., Zevnik, B., Anastassiadis, K., Niwa, H., Klewe-Nebenius, D., Chambers, I., Scholer, H.**
340 **and Smith, A.** (1998). Formation of pluripotent stem cells in the mammalian embryo
341 depends on the POU transcription factor Oct4. *Cell* **95**, 379-391.
- 342 **Niwa, H., Burdon, T., Chambers, I. and Smith, A.** (1998). Self-renewal of pluripotent embryonic
343 stem cells is mediated via activation of STAT3. *Genes Dev* **12**, 2048-2060.
- 344 **Ollion, J., Cochenec, J., Loll, F., Escude, C. and Boudier, T.** (2013). TANGO: a generic tool for high-
345 throughput 3D image analysis for studying nuclear organization. *Bioinformatics* **29**, 1840-
346 1841.
- 347 **Pietzsch, T., Saalfeld, S., Preibisch, S. and Tomancak, P.** (2015). BigDataViewer: visualization and
348 processing for large image data sets. *Nat Methods* **12**, 481-483.
- 349 **Silva, J., Nichols, J., Theunissen, T. W., Guo, G., van Oosten, A. L., Barrandon, O., Wray, J.,**
350 **Yamanaka, S., Chambers, I. and Smith, A.** (2009). Nanog is the gateway to the pluripotent
351 ground state. *Cell* **138**, 722-737.
- 352 **Smith, A. G., Heath, J. K., Donaldson, D. D., Wong, G. G., Moreau, J., Stahl, M. and Rogers, D.**
353 (1988). Inhibition of pluripotential embryonic stem cell differentiation by purified
354 polypeptides. *Nature* **336**, 688-690.
- 355 **Solter, D. and Knowles, B.** (1975). Immunosurgery of mouse blastocyst. *PNAS* **72**, 5099-5102.
- 356 **Takeda, K., Noguchi, K., Shi, W., Tanaka, T., Matsumoto, M., Yoshida, N., Kishimoto, T. and**
357 **Akira, S.** (1997). Targeted disruption of the mouse Stat3 gene leads to early embryonic
358 lethality. *Proc Natl Acad Sci U S A* **94**, 3801-3804.
- 359 **Tesar, P. J., Chenoweth, J. G., Brook, F. A., Davies, T. J., Evans, E. P., Mack, D. L., Gardner, R. L.**
360 **and McKay, R. D.** (2007). New cell lines from mouse epiblast share defining features with
361 human embryonic stem cells. *Nature* **448**, 196-199.
- 362 **Weitlauf, H. M. and Greenwald, G. S.** (1968). Survival of blastocysts in the uteri of ovariectomized
363 mice. *J Reprod Fertil* **17**, 515-520.
- 364 **Williams, R. L., Hilton, D. J., Pease, S., Willson, T. A., Stewart, C. L., Gearing, D. P., Wagner, E. F.,**
365 **Metcalf, D., Nicola, N. A. and Gough, N. M.** (1988). Myeloid leukaemia inhibitory factor
366 maintains the developmental potential of embryonic stem cells. *Nature* **336**, 684-687.
- 367 **Yamanaka, Y., Lanner, F. and Rossant, J.** (2010). FGF signal-dependent segregation of primitive
368 endoderm and epiblast in the mouse blastocyst. *Development* **137**, 715-724.
- 369 **Yan, H., Malik, N., Kim, Y. I., He, Y., Li, M., Dubois, W., Liu, H., Peat, T. J., Nguyen, J. T., Tseng, Y.**
370 **C., et al.** (2021). Fatty acid oxidation is required for embryonic stem cell survival during
371 metabolic stress. *EMBO Rep* **22**, e52122.
- 372 **Ye, S., Li, P., Tong, C. and Ying, Q. L.** (2013). Embryonic stem cell self-renewal pathways converge
373 on the transcription factor Tfcp2l1. *EMBO J* **32**, 2548-2560.
- 374 **Ying, Q. L., Wray, J., Nichols, J., Batlle-Morera, L., Doble, B., Woodgett, J., Cohen, P. and Smith,**
375 **A.** (2008). The ground state of embryonic stem cell self-renewal. *Nature* **453**, 519-523.

376 **Yoshida, K., Taga, T., Saito, M., Suematsu, S., Kumanogoh, A., Tanaka, T., Fujiwara, H., Hirata,**
377 **M., Yamagami, T., Nakahata, T., et al. (1996).** Targeted disruption of gp130, a common
378 signal transducer for the interleukin 6 family of cytokines, leads to myocardial and
379 hematological disorders. *PNAS* **93**, 407-411.
380 **Zhang, T., Kee, W. H., Seow, K. T., Fung, W. and Cao, X. (2000).** The coiled-coil domain of Stat3 is
381 essential for its SH2 domain-mediated receptor binding and subsequent activation induced
382 by epidermal growth factor and interleukin-6. *Mol Cell Biol* **20**, 7132-7139.
383
384

385 **Figure Legends**

386 *Figure 1. Distribution of pSTAT3(Y705) and TFPC2L1 in preimplantation and diapause embryos*

387 (A) Schematic of mouse reproductive system representing normal preimplantation development
388 (left) and induction of diapause (right). Diapause was induced by surgical removal of both ovaries
389 at E2.5 (before the physiological burst of oestrogen production) and embryos were collected 6
390 days later, thus being diapaused for 4 days. (B) Confocal images of NANOG, pSTAT3(Y705) and
391 TFPC2L1 IF in preimplantation E3.5, 4.5 and diapause embryos. Scale bar = 20 μ m.

392

393 *Figure 2. Development of analysis tool for pre-implantation mouse embryo IF*

394 (A) Schematic of image analysis pipeline to segment individual nuclei in 3D and quantify
395 fluorescence of each channel. The region of each embryo to be quantified is depicted by a dotted
396 red oval, thus excluding the mural trophectoderm region that does not participate in subsequent
397 formation of the foetus. (B) Representative example embryos from each developmental stage with
398 nuclei represented by a scatter point, and colour coded based on (STAT3)pY705 or TFPC2L1
399 integrated density. (C) Violin plots with overlaid boxplots of the integrated density of pY705 and
400 TFPC2L1 expression across each nucleus from each embryo by stage (E3.5, n = 29, E4.5, n= 33,
401 diapause, n = 54). Segmented nuclei were filtered for DAPI signal and volume to remove any
402 erroneous segmentation. * $P < 0.01$.

403

404 *Figure 3. Example of analysis of embryo IF*

405 (A) Nuclei are colour-coded by stage dispersed in a 3D co-expression space based on integrated
406 density (sum across all pixel values in the 3D object) of NANOG and pY705 and in each
407 segmented nucleus. The polygon selection encloses cells with a pY705 raw integrated density
408 above 5×10^5 . (B) Distribution of the selected high pY705 cells within the polygon from (A) in their
409 embryo of origin for 3 representative diapaused embryos (top) with all nuclei shown below. (C)
410 Representative example embryos from each developmental stage with nuclei represented by a
411 scatter point and colour coded based on pY705 integrated density.

412

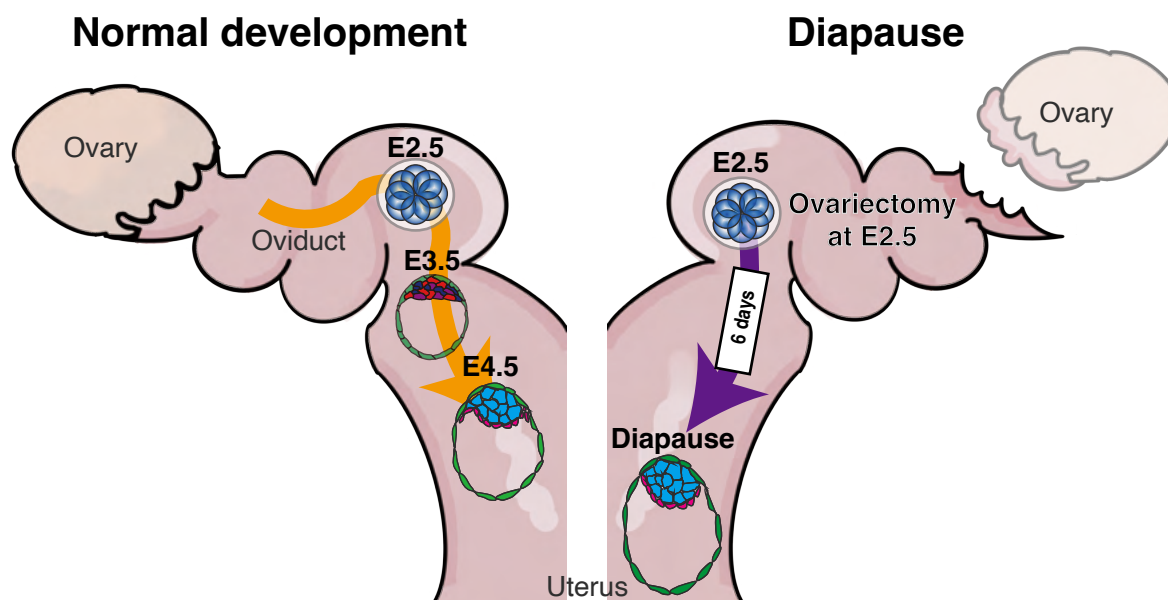
413 *Figure 4. STAT3 and TFPC2L1 are required for ICM maintenance during diapause, but STAT3 is*
414 *not required for ESC derivation or self-renewal*

415 (A, B) IF of NANOG, pY705 and TFPC2L1 in diapause for (A) *Stat3* WT/het and null embryos and
416 (B) *Tfcp2l1* WT/het and null embryos. Scale bar = 20 μ m. (C) Number of ICM cells in *Stat3* or
417 *Tfcp2l1* WT/Het and null diapause embryos. (D) Bright field images of WT and *Stat3* null ESCs.
418 Scale bar = 100 μ m. (E) Proliferation based on cell number counts of WT and *Stat3* null ESCs
419 cultured in N2B27+2i medium for 5 days (day4: $p=0.14$, day5: $p=0.55$ by Student's T test). (F)
420 Immunofluorescence of OCT4 and NANOG in WT and *Stat3* null ESCs. Scale bar = 100 μ m.

421

Figure 1

A bioRxiv preprint doi: <https://doi.org/10.1101/2022.09.23.509173>; this version posted September 23, 2022. The copyright holder for this preprint (which was not certified by peer review) is the author/funder. All rights reserved. No reuse allowed without permission.



B

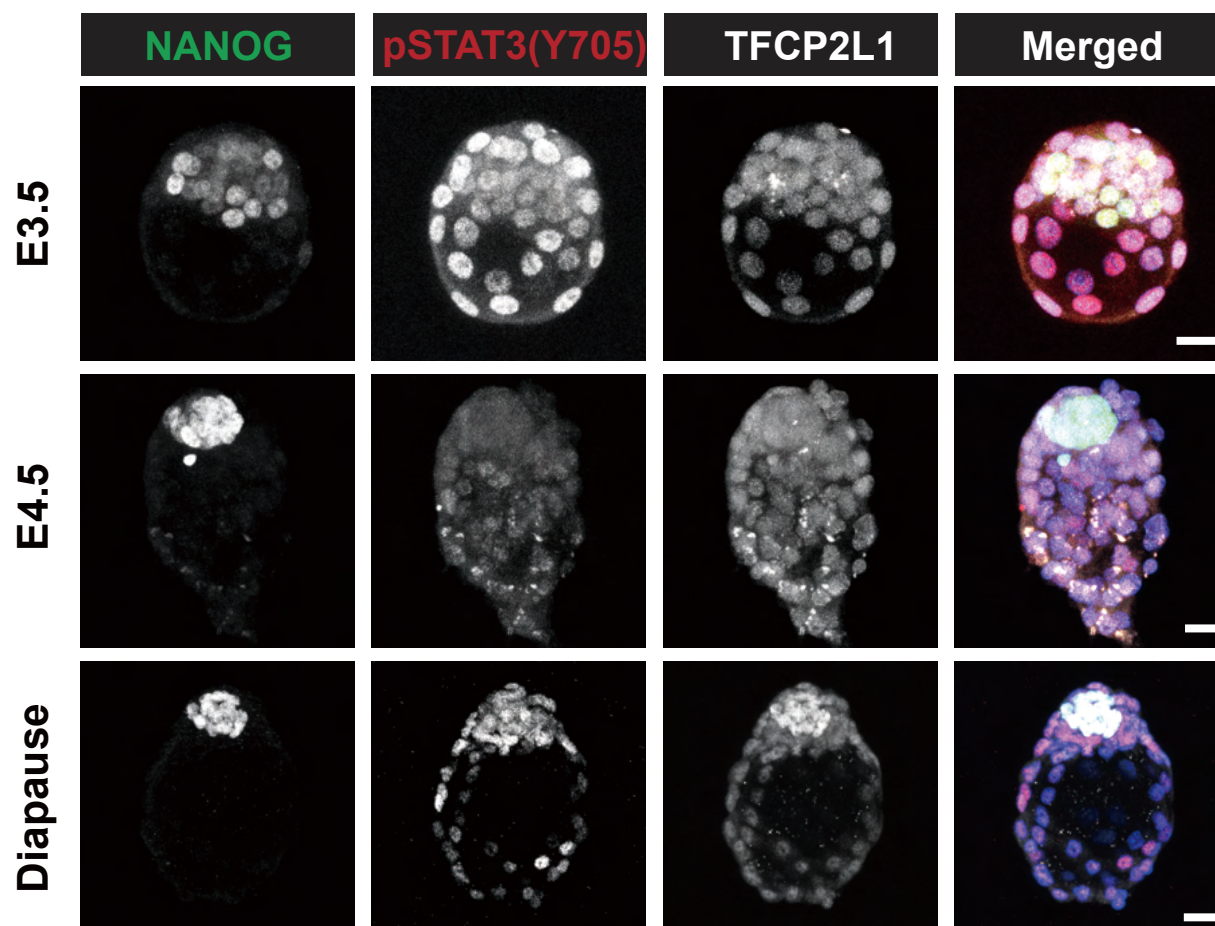
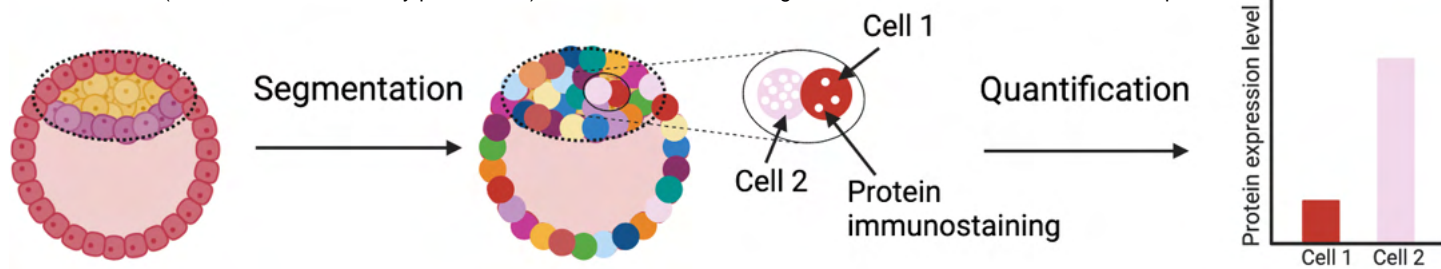


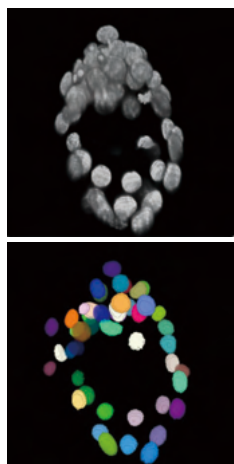
Figure 2

A

bioRxiv preprint doi: <https://doi.org/10.1101/2022.09.23.509173>; this version posted September 23, 2022. The copyright holder for this preprint (which was not certified by peer review) is the author/funder. All rights reserved. No reuse allowed without permission.



B



C

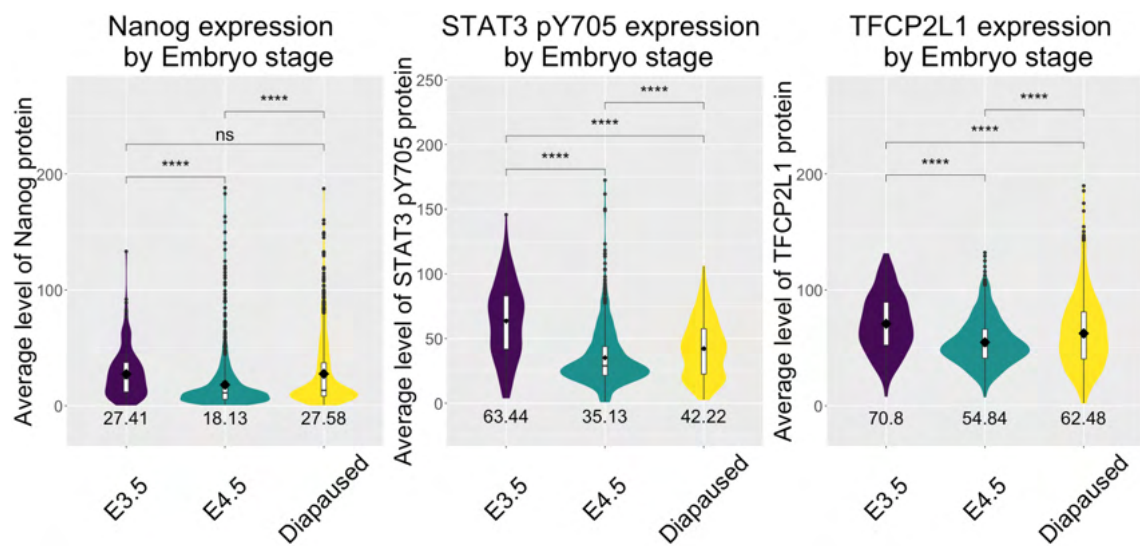
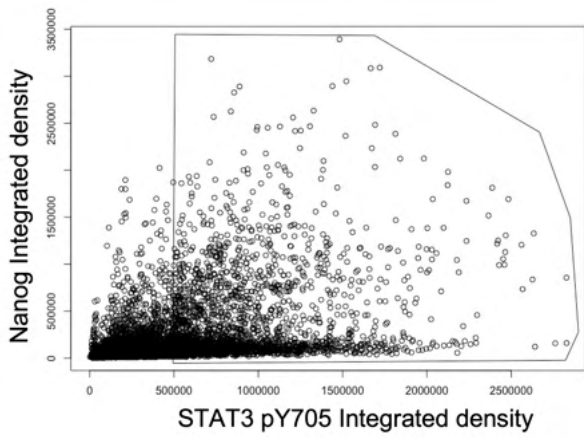


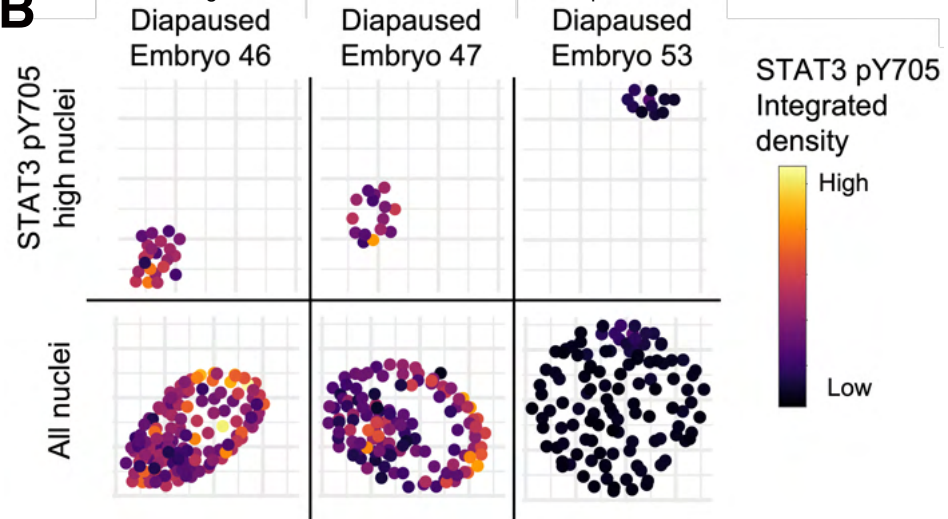
Figure 3

bioRxiv preprint doi: <https://doi.org/10.1101/2022.09.23.509173>; this version posted September 23, 2022. The copyright holder for this preprint (which was not certified by peer review) is the author/funder. All rights reserved. No reuse allowed without permission.

A



B



C

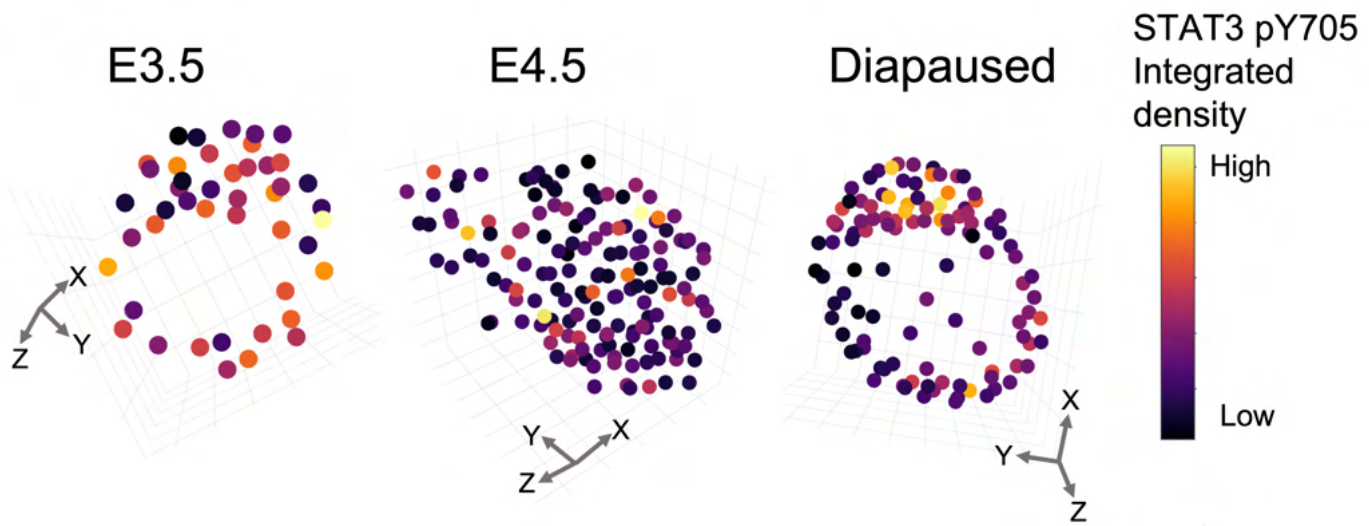
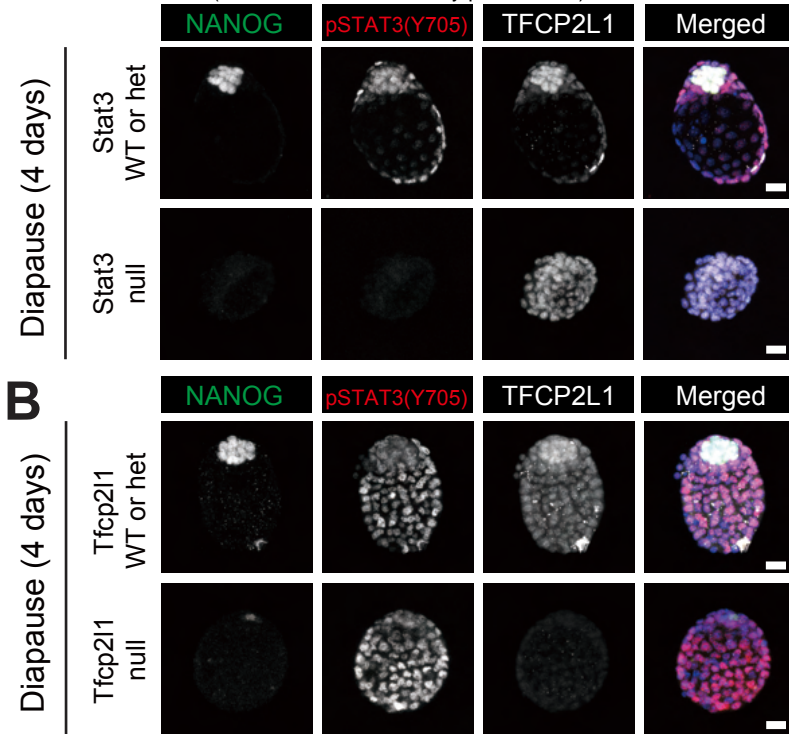


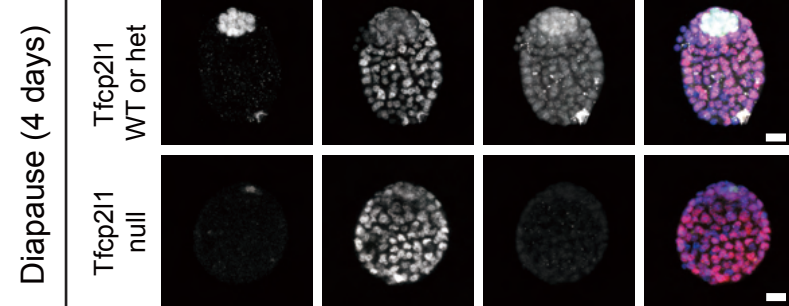
Figure 4

A

bioRxiv preprint doi: <https://doi.org/10.1101/2022.09.23.509173>; this version posted September 23, 2022. The copyright holder for this preprint (which was not certified by peer review) is the author/funder. All rights reserved. No reuse allowed without permission.

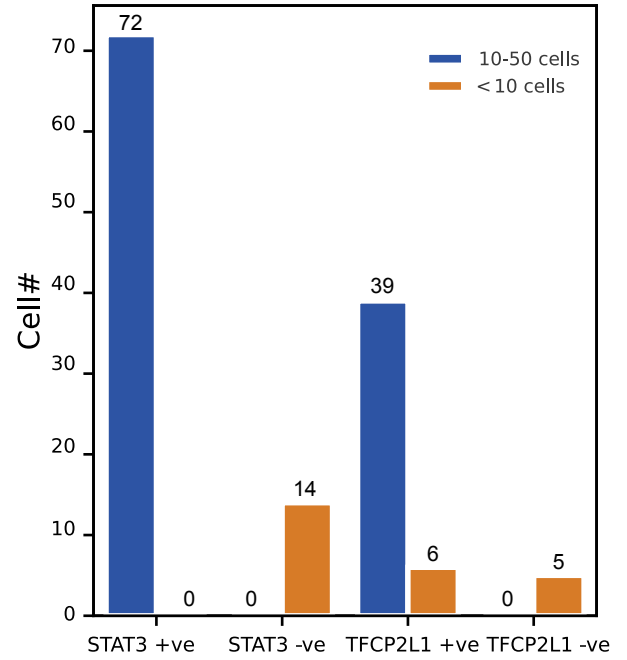


B

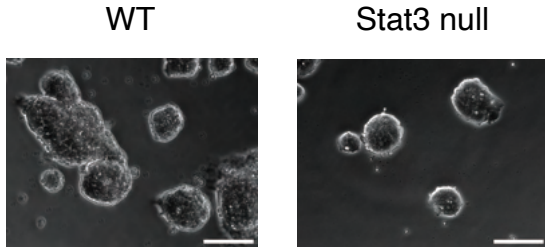


C

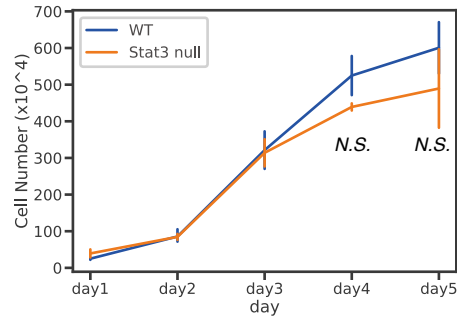
ICM cells in STAT3 blastocysts DIAPAUSE (4 days)



D



E



F

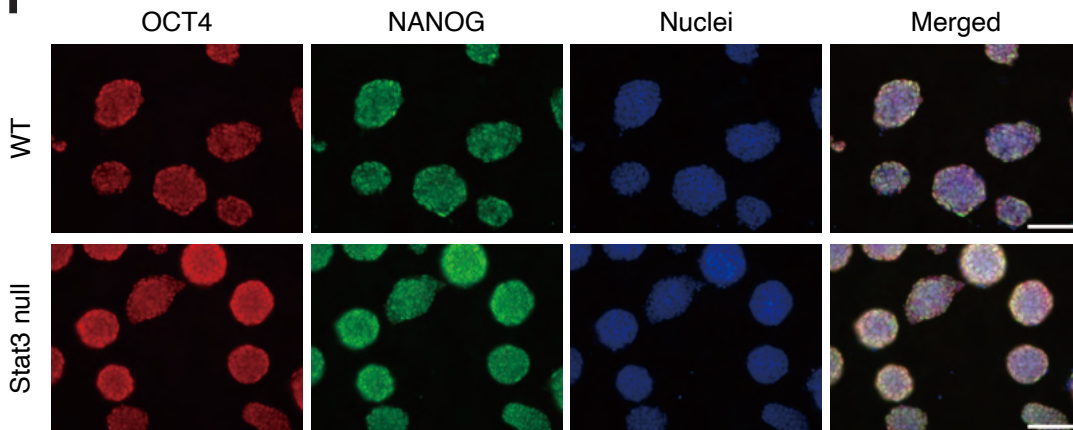


Table 1

ESCs derivation from ICM of Stat3 or Tfcp2l1 heterozygous intercrosses

bioRxiv preprint doi: <https://doi.org/10.1101/2022.09.23.509173>; this version posted September 23, 2022. The copyright holder for this preprint (which was not certified by peer review) is the author/funder. All rights reserved. No reuse allowed without permission.

	+/+ or +/-	-/-	Total ICM
Stat3	41	13	56
Tfcp2l1	55	0	65